J Mater Sci (2010) 45:557–561
DOI 10.1007/s10853-009-3976-8

Thermal and structural study of nanocrystalline Fe(Co)NiZrB alloys prepared by mechanical alloying

A. González · L. Escoda · J. J. Suñol · G. Shao · B. Arcondo · P. Bruna

Received: 10 February 2009 / Accepted: 12 October 2009 / Published online: 24 October 2009

Abstract Three nanocrystalline alloys, $Fe_{75-x}Co_x(Ni_{70}Zr_{30})_{15}B_{10}$ ($x = 0$, 10, and 20), were synthesized from elemental powders in a planetary high-energy ball mill. Their microstructure, magnetic properties, and thermal stability were characterized by X-ray diffraction, transmission Mössbauer spectroscopy, transmission electron microscopy, scanning electron microscopy, induction coupled plasma, vibrating sample magnetometry, and differential scanning calorimetry. After 80 h of milling, the nanocrystallites size of alloys is in the range 6–10 ± 1 nm. The lattice parameter decreases when increasing (decreasing) milling time (Fe content). Furthermore, the thermal stability of the nanocrystalline phase increases when increasing Co concentration. The activation energy of the main crystallization process, between 275 ± 8 and 311 ± 10 kJ mol^{-1}, is associated with grain growth. Slight contamination from milling tools and milling atmosphere was detected. Minor differences were detected after Mössbauer analysis.

A. González · L. Escoda · J. J. Suñol (✉)
Department de Fisica, Universitat de Girona,
Campus Montilivi, Girona 17071, Spain
e-mail: joanjosep.sunyol@udg.edu

G. Shao
Brunel University, BCAST, Uxbridge UB8 3PH, Middex, UK

B. Arcondo
Lab Solidos Amorfos, Universitat Buenos Aires,
Buenos Aires, DF RA-1063, Argentina

P. Bruna
EPSC, UPC, Avda. Canal Olímpic s/n,
Castelldefels 08860, Spain

Introduction

In the last decades, it has been proved that non-equilibrium phases such as amorphous, quasicrystalline, and nanocrystalline can be prepared by means of the mechanical alloying (MA) process [1–4]. During mechanical alloying, powder particles are subjected to severe mechanical deformation by collision with milling media and are repeatedly deformed, cold-welded and fractured, favoring diffusion. Nanocrystalline materials have attracted considerable interest due to their interesting technological applications including ductile ceramics, hydrogen storage materials, and unusual magnetic behavior [5, 6]. Particularly, nanocrystalline Fe–(Zr, Nb)–B alloys containing bcc-Fe nanocrystallites are of interest as soft magnetic materials [7, 8]. The substitution of small amounts of Co or Ni for Fe in Fe-based magnetic materials generally results in an increase of saturation magnetization [9]. Furthermore, it is known that the use of Ni favors the development of metastable structures at low milling times [10]. The purpose of this study is to analyze the structural and thermal changes induced by partial substitution of Fe by Co in nanocrystalline Fe(Co)-based alloys produced by MA.

Experimental procedure

The alloys were prepared by milling elemental Fe, Co, B and prealloyed Zr–Ni powders (purity of 99.9% or more and particle size below 125 μm) in a planetary ball mill (Fritsch P7) using stainless steel balls and vials (capacity: 50 mL). The milling was performed at 700 rpm (disk and vials) under Ar atmosphere. The ball-to-powder mass ratio was 5:1. Powder extractions for analysis were carried out after 10, 20, 40, and 80 h of MA. Three alloys

were produced: $Fe_{75-x}Co_x(Ni_{70}Zr_{30})_{15}B_{10}$ ($x = 0$, 10, and 20 at.%) and labeled as A, B, and C, respectively.

The structural analysis was performed by X-ray diffraction (XRD) using a D-500 Siemens equipment with Cu K_α radiation. The analyses of the patterns were performed using the Rietveld refinement with the MAUD program [11]. Complementary observation and analysis were performed with transmission scanning microscopy (TEM) on a CM200 Philips microscope. Magnetic measurements were performed using a vibrating sample magnetometer (VMS) in a Lake-Shore device. Transmission Mössbauer spectra were measured with a conventional spectrometer working at room temperature and using a 25 mCi source of ^{57}Co in a Rh matrix. The samples' thermal characterizations were carried out by differential scanning calorimetry (DSC) under an argon atmosphere in a Mettler-Toledo's DSC822 equipment. DSC experiments were performed at heating rates ranging from 2.5 to 40 K/min. The morphology and composition study were performed with scanning electron microscopy (SEM) on a DSM960A Zeiss microscope with energy dispersive X-ray microanalysis (EDX) and with induced coupled plasma (ICP) on a Liberty-RL ICP Varian spectrometer.

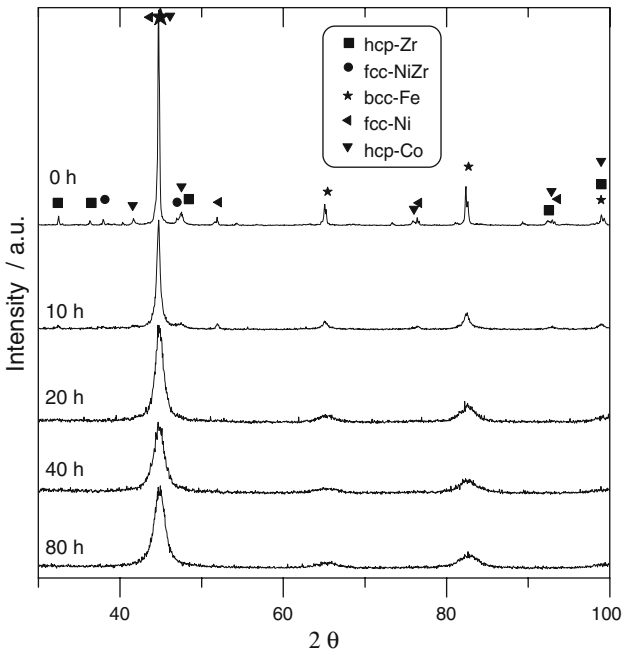

Fig. 1 XRD patterns of alloy C milled at different milling times: *a* 0 h, *b* 10 h, *c* 20 h, *d* 40 h, and *e* 80 h

Results and discussion

The formation of the nanocrystalline structure during mechanical alloying was followed by X-ray diffraction. As the milling time increases, the peaks due to minor phases disappear while the bcc-Fe peaks broaden and their intensities decrease. As an example, Fig. 1 shows the XRD spectra corresponding to the alloy C at different milling times. The solid solution is formed after 20–40 h of milling. Milling for longer times can favor the homogeneity of the solid solution formed. The resultant diffraction spectra were analyzed using the Rietveld method, see Table 1. The final structure of the materials is a Fe-rich bcc solid solution. The general trend is an increase (decrease) of lattice strain (crystal size) when increasing the milling time. The nanocrystallites formed after 80 h of milling were about 6–10 ± 1 nm in average size. The lowest value corresponds to alloy A (alloy without Co). The lattice strain observed, between 0.687 ± 0.008 and 0.755 ± 0.008% at 80 h, is in concordance with typical values of distorted lattices. To analyze the milling process, the representation of the internal lattice strain versus the reciprocal crystallite size is shown in Fig. 2. In a first step, there is a diminution of the crystallite size and an increase of the internal lattice strain. In a second step, the internal stress increases with milling time whereas crystallite size remains nearly constant. An increase of the lattice strain index indicates an increase in the density of crystallographic defects [12]. The lattice parameter values of the bcc-Fe solid solution are influenced by other alloys components especially after longer milling.

Micrographs obtained by transmission electron microscopy confirm the existence of zones with a nanometric structure. As an example of characteristic TEM images of these alloys, Fig. 3 shows micrographs corresponding to alloy A milled for 80 h with three selected zones corresponding to nanocrystals with 5–10 nm in size, in concordance with XRD results.

Complementary structural analysis was performed by Transmission Mössbauer spectroscopy. All the spectra were fitted using a magnetic hyperfine field histogram distribution and the Hesse-Rübartsch method, including a linear correlation between the isomer shift and the magnetic field. Figure 4 shows the TMS spectra and Mössbauer parameters are given in Table 2. All samples show the sextet associated to bcc-Fe-rich solid solutions. Usually, Co introduction increases the hyperfine magnetic field and the introduction of non-magnetic elements diminishes it. Furthermore, two minority paramagnetic phases are necessary to adjust the Mössbauer spectra of alloy without Co. This interaction is a one-peak distribution, probably corresponding to a low moment (LM) Fe-rich FCC phase called antitaenite [13] with isomer shift IS = 0.02 mm/s, and a doublet with hyperfine parameters IS ≈ 0.24 mm/s and quadrupolar splitting QS ≈ 0.34 mm/s. Figure 5 shows the hyperfine field distributions of alloys milled during 80 h. The peak position is higher than 33.1 T (value

Table 1 Microstructural parameters of $Fe_{75-x}Co_x(Ni_{70}Zr_{30})_{15}B_{10}$ ($x = 0$, 10, and 20) powders corresponding to bcc-Fe-rich solid solution

Time (h)	A ($x = 0$)			B ($x = 10$)			C ($x = 20$)		
	A (nm) $\pm 3 \times 10^{-4}$	L (nm) ± 1	$\langle\sigma^2\rangle^{1/2}\%$ $\pm 8 \times 10^{-3}$	A (nm) $\pm 3 \times 10^{-4}$	L (nm) ± 1	$\langle\sigma^2\rangle^{1/2}\%$ $\pm 8 \times 10^{-3}$	A (nm) $\pm 3 \times 10^{-4}$	L (nm) ± 1	$\langle\sigma^2\rangle^{1/2}\%$ $\pm 8 \times 10^{-3}$
10	0.2867	10	0.154	0.2867	16	0.135	0.2866	15	0.187
20	0.2875	8	0.248	0.2867	10	0.506	0.2860	13	0.667
40	0.2873	7	0.709	0.2865	8	0.765	0.2856	9	0.690
80	0.2865	6	0.704	0.2864	8	0.755	0.2858	10	0.687

The errors given are an upper limit

A lattice parameter, *L* crystallite size, $\langle\sigma^2\rangle^{1/2}$ lattice strains

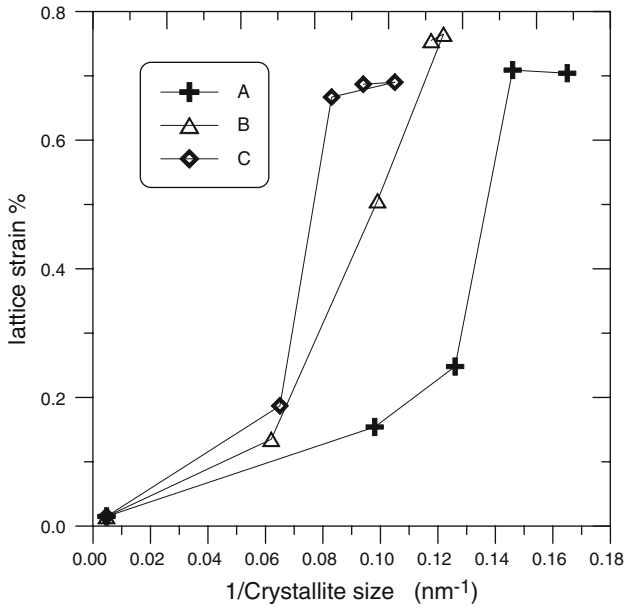

Fig. 2 XRD parameters evolution. Relation between crystallite size and internal lattice strain

corresponding to bcc-Fe) due to solid solution in this multicomponent system [14]. Furthermore, alloys with Co have a wider peak probably due to a poor homogeneity of the solid solution (especially in alloy C). This fact can explain the lower value of average magnetic field of alloy C (20% Co) if compared with alloy B (10% Co).

The magnetic properties of as milled alloys, i.e., coercivity H_c and saturation magnetization M_s for 80 h of milling are given in Table 3. The saturation magnetization increases as increasing the Co content. The values change from 108 to 123 emu/g. Furthermore, a slight increase on the coercivity was also found (from 95 to 104 Oe). Similar values were found in a $Fe_{60}Co_{10}(Ni_{70}Zr_{30})_{15}B_{15}$ alloy [15].

The general characters of the DSC traces for all compositions are similar. Figure 6 shows the results corresponding to alloys A, B, and C milled for 80 h. The broad exothermic process starting at ~420–450 K might be due to the relief of internal stress [16, 17]. In all alloys, two additional exothermic processes were detected: a low-temperature process beginning at ~600 K, and the main process beginning at ~800 K. The apparent activation energies, *E*, for the crystallization processes of alloys were evaluated using the Kissinger method. For the first process, the values obtained, between 146 ± 5 and 154 ± 7 kJ/mol, can be associated to early surface crystallization (particle surface) of the nanocrystalline phase obtained after milling, and also to the relief of internal stress [18]. The

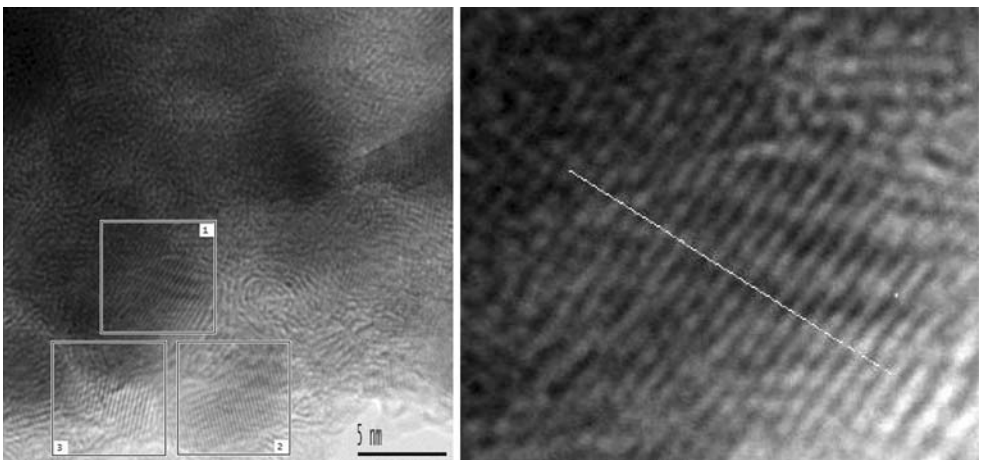

Fig. 3 TEM micrograph corresponding to alloy A

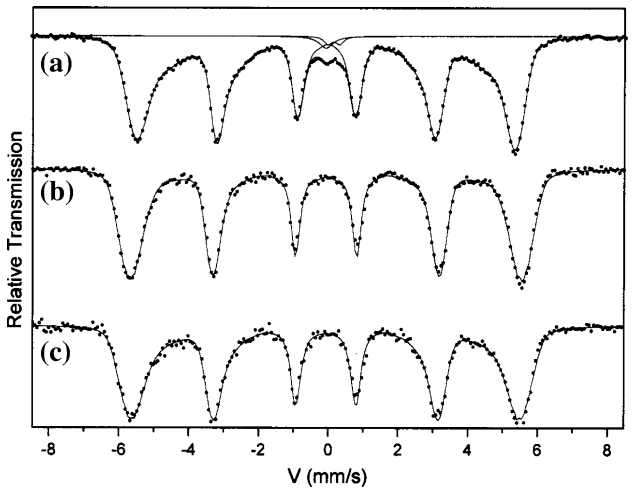

Fig. 4 Mössbauer spectra corresponding to alloys milled for 80 h

Table 2 Mössbauer parameters: average hyperfine magnetic field (BHF), isomer shift (IS), and quadrupolar splitting (QS)

Simple	Phase	BHF/T	IS/mm s^{-1}	QS/mm s^{-1}	Area (%)
A	Bcc-Fe-rich	31.1(2)	0.04(1)	−0.02(1)	96
	Doublet	–	0.02(1)	–	2
	Singlet	–	0.24(1)	0.34(1)	2
B	Bcc-Fe-rich	33.1(1)	0.029(3)	−0.002(3)	100
C	Bcc-Fe-rich	32.4(2)	0.029(1)	−0.005(3)	100

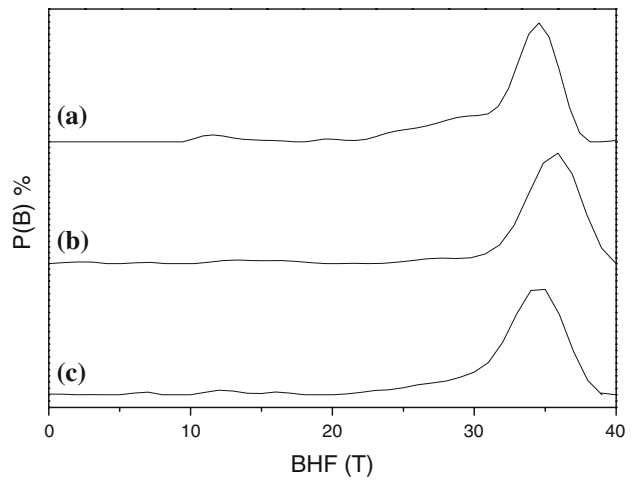

Fig. 5 Hyperfine field distributions corresponding to alloys milled for 80 h

Table 3 Magnetic properties of alloys milled during 80 h

Time (h)	A ($x = 0$)		B ($x = 10$)		C ($x = 20$)	
	M_s (emu/g)	H_c (Oe)	M_s (emu/g)	H_c (Oe)	M_s (emu/g)	H_c (Oe)
80	108	95	114	97	123	104

M_s saturation magnetization, H_c coercivity

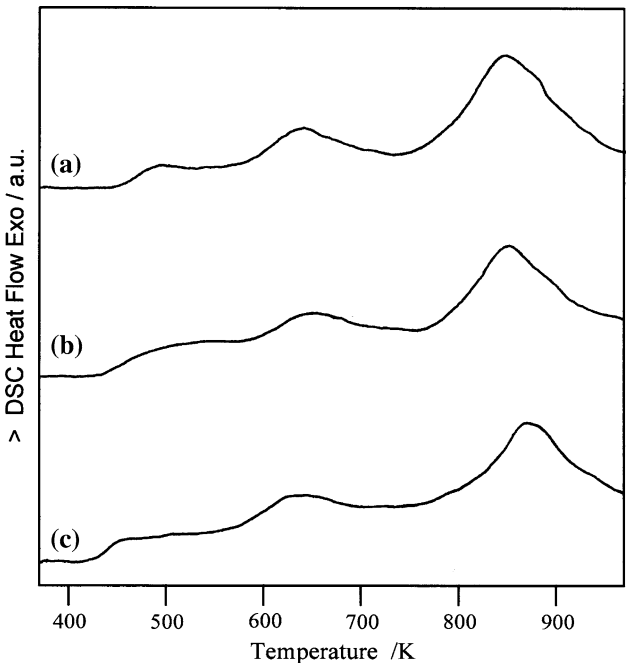

Fig. 6 DSC scans corresponding to alloys milled for 80 h

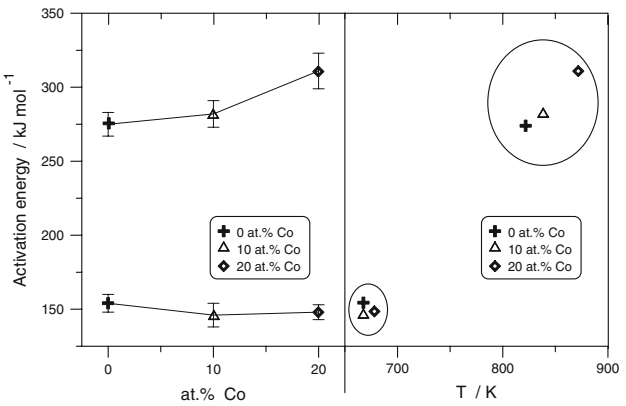

Fig. 7 Apparent activation energies obtained from Kissinger method of the crystallization process detected in DSC scans of alloys milled for 80 h: as a function of Co content (*left*) and as a function of peak temperature (*right*)

values obtained for the main phase, between 275 ± 8 and 311 ± 10 kJ mol^{-1}, can reasonably be associated with a grain growth process [19]. Similar values were found in alloys with similar composition [20]. Thermal stability is associated with high activation energy and crystallization temperature. Figure 7 shows activation energy as a function of Co at.% (left) and as a function of the peak crystallization temperature (right). The nanostructure of alloy C after 80 h of milling (containing 20 at.% Co) is the most stable front the grain growth process (higher activation energy and peak temperature).

The contamination measured by EDX and ICP in the powdered alloys increases with milling time. Nevertheless, the results show only slight (<0.6 at.%) contamination from Cr in all alloys after 80 h of MA. Similar results are reported in other Fe-rich alloys [21, 22], whereas other authors found higher contamination from milling tools [23]. Contamination is similar in all samples and its influence is probably negligible in the structural and thermal differences detected.

Conclusions

Several nanocrystalline alloys, $Fe_{75-x}Co_x(Ni_{70}Zr_{30})_{15}B_{10}$ (with $x = 0$, 10, and 20 at.%) were produced after 80 h of mechanical alloying. The partial substitution of Fe by Co favors the formation of a Fe-rich nanocrystalline alloy with high thermal stability regarding crystalline growth (by increasing both the temperature and the activation energy of the main crystallization process). Furthermore, the saturation magnetization increases as increasing the Co content (from 108 to 123 emu/g). From XRD analysis, the mean crystallite size of the bcc-Fe-rich solid solution ranges between 6 ± 1 (alloy without Co) and 10 ± 1 nm as determined by XRD and TEM. The crystallite size and lattice strain analysis show the presence of several steps: diminution of the crystallite size and increasing of the internal lattice strain and an increase of internal stress whereas crystallite size remains nearly constant.

Acknowledgements Financial support from MICYT MAT2006-13925-C02-02 (FEDER) and DURSI 2005SGR-00201 projects is acknowledged.

References

1. Suryanarayana C (2001) Prog Mater Sci 46:1
2. Nasu T, Nagaoka K, Itoh N, Suzuki K (1990) J Non Cryst Solids 122:216
3. Chiriac H, Moga AE, Urse M, Hison C (2000) J Metastable Nanocryst Mater 8:806
4. Amini R, Hadianfard MJ, Salahinejad E et al (2009) J Mater Sci 44:136. doi:10.1007/s10853-008-3117-9
5. Kalisvaart WP, Notten PHL (2008) J Mater Res 23:2179
6. McHenry ME, Willard MA, Laughlin DE (1999) Prog Mater Sci 44:291
7. Stiller C, Eckert J, Roth S et al (1996) J Non Cryst Solids 207:620
8. Garataonandia JS, Gorria P, Fernández-Barquín L et al (2000) Phys Rev B 26:1650
9. Jang YI, Kim J, Shin DH (2000) J Mater Sci Eng B 78:113
10. Lee BH, Ahn BS, Kim DG et al (2003) Mater Lett 57:1103
11. Ferrari M, Lutterotti L (1990) J Appl Phys 76(11):7246
12. Shao YH, Sheng HW, Fu K (2001) Acta Mater 49:365
13. Abdu YA, Annersten H, Ericsson T et al (2004) J Magn Magn Mater 280:243
14. Moumeni H, Alleg S, Greneche JM (2005) J Alloys Compd 286:12
15. Pilar M, Escoda L, Suñol JJ et al (2008) J Magn Magn Mater 320:823
16. Calka A, Radlinski AP (1987) Acta Metall 35:1823
17. Suñol JJ, Pradell T, Clavaguera N et al (2003) Philos Mag 83(20):2323
18. Suñol JJ, González A, Saurina J et al (2007) J Non Cryst Solids 353:865
19. Multigner M, Hernando A, Crespo P et al (1999) J Magn Magn Mater 197:214
20. González A, Suñol JJ, Escoda L et al (2005) J Therm Anal Calorim 80:253
21. Malhouroux-Gaffet N, Gaffet E (1993) J Alloys Compd 198:143
22. González A, Bonastre J, Escoda L et al (2007) J Therm Anal Calorim 87:225
23. Domínguez-Crespo MA, Plata-Torres M, Torres-Huerta AM et al (2006) Mater Charact 56:138